Adv. Radio Sci., 21, 15–23, 2023
https://doi.org/10.5194/ars-21-15-2023

Advances in
Radio Science
Open Access Proceedings

Systematic methods for the synthesis of equidistant MIMO arrays

Marvin Alexander Samuel Holder[1] **and Mark Eberspächer**[2,1]

[1]Balluff GmbH, 73765 Neuhausen auf den Fildern, Germany
[2]Faculty of Electrical Engineering, Technical University of Applied Sciences Würzburg-Schweinfurt, 97421 Schweinfurt, Germany

Correspondence: Marvin Alexander Samuel Holder (marvin.holder@balluff.de)

Received: 1 February 2023 – Revised: 6 April 2023 – Accepted: 11 April 2023 – Published: 1 December 2023

Abstract. Finding a feasible antenna arrangement for *multiple input multiple output* (MIMO) arrays to serve a specific purpose is a first crucial step towards a successful MIMO radar system design. Design methods to synthesize uniformly weighted and equidistant MIMO arrays are proposed and investigated. The methods can be used to gain a design foundation for 1D or 2D arrays without software tools or programming effort. Since the presented approach does not consider electromagnetic fields, electromagnetic full-wave simulations might be required additionally. The method is based on sequentially copying and displacing antenna groups with the help of a number scheme. A nomenclature is proposed to classify the degrees of freedom in the design procedure. If the antennas are aligned to a uniform grid, a polynomial representation of the array can be chosen alternatively. This method is beneficial when redundancies of a produced array and where they appear must be analyzed. A new design problem arises when an array is to consist of only transceiving antennas, which can be analyzed with polynomial multiplication. One strategy to find a suitable MIMO array consisting of transceiver elements is given and evaluated.

1 Introduction

Using a *multiple input multiple output* (MIMO) array in radar applications can significantly reduce the number of required physical antennas of a radar system. This reduces the system complexity and can have economic advantages. In the radar domain, MIMO arrays are used in several applications and fields. Feger et al. (2009) use a non-uniform prototype MIMO array for far field 2D imaging and show potential applicability of their design in automotive scenarios. Other examples are public security scanning (e.g., Gao et al., 2018; Zhuge and Yarovoy, 2011) or package control (Yanik et al., 2020), where the penetrability of materials like textiles or cardboard is exploited. By using individual *transmitter* (Tx) and *receiver* (Rx) channels, each combination of them yields a full radar return signal. Therefore, the number of required physical antennas can be reduced. From a model point of view, a Tx-Rx pair can be modeled as a *virtual element* (VE). All antenna pairs of each combination result in a *virtual array* (VA). To analyze a structure of Tx and Rx antennas, the method of convolution and scaling is commonly used (Ender and Klare, 2009). However, for the synthesis of a VA, no straightforward method exists. Generic non-uniform MIMO arrays are useful to compromise resolution, sidelobe-levels and element-density in a controllable way. A suitable non-uniform array can be found by discrete optimization algorithms like particle swarm optimization (Schmid et al., 2009) or genetic algorithms (Huang et al., 2021). The signal processing for non-uniform arrays is computationally more complex in general, since no geometric structure can be exploited. On the other hand, efficient FFT-based methods can be used for uniform arrays, e.g. as given by Sheen et al. (2001) for 3D imaging. A specific type of MIMO arrays are the ones having equidistant virtual elements without overlapping items or gaps. When using uniform MIMO arrays for near-field imaging, signal corrections might be necessary to achieve the desired reconstruction accuracy (Yanik and Torlak, 2019). For a radar signal processing algorithm that fully relies on the virtual antenna concept, these overlapping VEs would deliver redundant information and the physical resources would not be exploited optimally in the sense of amount of elements. In this paper, a design method for equidistant MIMO arrays is introduced.

Published by Copernicus Publications on behalf of the URSI Landesausschuss in der Bundesrepublik Deutschland e.V.

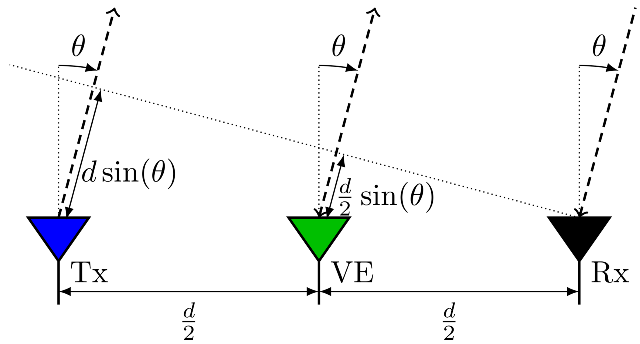

Figure 1. Virtual antenna resulting from a single Tx-Rx pair.

If the used antenna type is a so-called *transceiver* (TRx) (antenna which can act as both transmitter and receiver), redundant VEs are not avoidable. To analyze this more involved design problem, a polynomial representation of the design problem is introduced. One possible synthesis procedure for TRx antennas is described and rated in different aspects.

The remainder of the paper is structured as follows: Sect. 2 explains the concept of a virtual array and the method of convolution and scaling. Section 3 introduces the proposed design method for equidistant MIMO arrays. In Sect. 4, an example design for a 2D MIMO array is shown. Section 5 explains the polynomial representation and introduces an iterative method to synthesize a MIMO array consisting of TRx elements. Finally, Sect. 6 concludes the paper and gives an outlook on future work.

2 Virtual arrays

In this section, the concepts of a virtual antenna and a virtual array are explained.

2.1 Single transmitter-receiver pair

In a bistatic radar scenario, Tx and Rx are distinct antennas at different locations. If the distance R to a target is large compared to the distance d between both antennas, the geometric relationship can be simplified as shown in Fig. 1. The elevation angle θ is the same for both Tx and Rx. The total path L_{bi} of a plane wave is then

$$L_{\mathrm{bi}} = R + (R + d\sin(\theta)). \tag{1}$$

An imagined monostatic antenna midway between Tx and Rx leads to the same total pathlength. This relation also holds for an azimuth angle ϕ unequal to zero. For a large relative target distance R, the Tx-Rx pair can therefore be viewed as a virtual monostatic antenna (Chen and Vaidyanathan, 2009), a so-called *virtual element* (VE).

2.2 Convolution and scaling

If several Rx and Tx are used together, they form a MIMO system. To allow for the separation from different Tx after reception, the antennas are fed with orthogonal waveforms. Examples of orthogonal waveform strategies are *time division multiplex* (TDM) (Ender and Klare, 2009) and *orthogonal frequency division multiplex* (OFDM) (Krieger et al., 2008). Each of the N_{Rx} receiver antennas is able to separate the target responses from the N_{Tx} transmitter antennas. Therefore, each of the $N_{\mathrm{Tx}} \cdot N_{\mathrm{Rx}}$ combinations results in a VE, together forming a VA. To analyze the structure of a VA, the method of convolution and scaling can be used. First, the Rx and Tx antenna distributions are expressed as continuous spatial functions F_{Rx} and F_{Tx}, respectively. These functions possess Dirac spikes at the positions, where an antenna is located. Second, as shown in Ender and Klare (2009), the virtual antenna array is now calculated by convolving scaled versions of the two functions

$$F_{\mathrm{VA}}(x, y) = F_{\mathrm{Tx}}(2x, 2y) * F_{\mathrm{Rx}}(2x, 2y), \tag{2}$$

where $(*)$ denotes a 2D convolution.

3 Design method for one-dimensional equidistant arrays

The main focus of this paper is to introduce a simple design method for an equidistant and equally weighted VA along x. Such a VA has the form

$$F_{\mathrm{VA}}(x, y_{\mathrm{VA}}) = \sum_{i=0}^{L-1} 1 \cdot \delta(x - k \cdot i, y_{\mathrm{VA}}) \tag{3}$$

with size L and a scaling factor k. The overall length of the VA is $k(L-1)$. The VA forms a grid along x at y_{VA}. Note, that each element in the sum has a weighting of 1, which means exactly one Tx-Rx pair contributes to this VE location. To obtain functions F_{Tx} and F_{Rx}, a straightforward method is explained in the following sections.

3.1 Establishment of requirements

In order to generate a regular MIMO array in the required form of Eq. (3) with size L, the prime factorization of L is done first. The P prime factors $p_i \in \mathbb{N}$ with the property

$$L = \prod_{i=0}^{P-1} p_i \tag{4}$$

themselves are of course primes and cannot be divided further. It is recommended to choose L, such that the prime factors p_i will not get too large. This adds more design flexibility in the method.

3.2 Theoretical outline

From this point onwards, a mixed basis number system will be introduced. Unlike the well-known decimal, binary or hexadecimal number systems, each digit is assigned its own basis. The number system will be represented by a W-element sequence of numbers $\langle \alpha_0, \alpha_1, \ldots, \alpha_{W-1} \rangle$, where $\langle \cdot \rangle$ denotes an ordered, finite sequence of numbers and α_i the base of the digit at position i, e.g., a three-digit number with basis $\langle 4, 3, 2 \rangle$ will have a binary least significant digit. The most significant digit has base 4 and the one in between is ternary. Counting in this number system would yield $000, 001, 010, 011, 020, \ldots, 320, 321$. As seen, the amount of displayable numbers in such a number system is finite. A number y in a mixed basis system can be represented as a concatenation of W symbols in the form

$$y = d_0 d_1 \ldots d_{W-1} \in \mathbb{S}_S, \quad d_i \leq \alpha_i - 1, \tag{5}$$

where $\mathbb{S}_S$ denotes the set of all displayable numbers in a number system S. The conversion $\mathtt{conv}(y; S)$ of an integer y from a number system S into a decimal z is calculated as

$$z = \mathtt{conv}(y; S) = d_{W-1} + \sum_{i=0}^{W-2} d_i \cdot \left(\prod_{j=i+1}^{W-1} \alpha_j \right). \tag{6}$$

Next, each prime factor is either assigned a subscript t for Tx or a r for Rx. This can be notated as

$$\left(p_i \leftarrow p_{i,t}\right) \oplus \left(p_i \leftarrow p_{i,r}\right) \quad \forall i \in \mathbb{N} < W, \tag{7}$$

where $\oplus$ denotes a logical exclusive or operation. The sequence $\mathcal{P}$ is defined as an ordered list of the annotated prime factors in the form

$$\mathcal{P} = \left\langle p_{0,[t|r]}, p_{1,[t|r]}, \ldots, p_{P-1,[t|r]} \right\rangle. \tag{8}$$

$[t|r]$ denotes, that either the subscript t or r is chosen for each element, but not both. Note, that the choice of a particular assignment as well as the order of the prime factors in $\mathcal{P}$ will influence the inner structure of the resulting VA and should be chosen in such a way as to design the most feasible MIMO array. A particular number system S with the ordered prime factors from Eq. (8) is now considered. It is in the form

$$S = \langle p_0, p_1, \ldots, p_{P-1} \rangle \tag{9}$$

with $P = W$. For the Tx and Rx antennas, sets of enumerated numbers $\mathcal{T}_\mathrm{x}$ and $\mathcal{R}_\mathrm{x}$ in the number system of Eq. (9) are created respectively. Therefore, the assignment of subscripts t and r from Eq. (8) is used. For $\mathcal{T}_\mathrm{x}$ all possible numbers in the number system are listed, where the digits at locations with $p_{i,r}$ are zero. For $\mathcal{R}_\mathrm{x}$ respectively, all possible numbers are listed of which the digits d_i are zero, if $p_i \leftarrow p_{i,t}$. Formally, this can be written as

$$\mathcal{T}_\mathrm{x} = \left\{ x \in \mathbb{S}_S | p_i \leftarrow p_{i,r} \Rightarrow d_i = 0 \right\} \tag{10}$$

and

$$\mathcal{R}_\mathrm{x} = \left\{ x \in \mathbb{S}_S | p_i \leftarrow p_{i,t} \Rightarrow d_i = 0 \right\}. \tag{11}$$

The number of elements in $\mathcal{T}_\mathrm{x}$ is given by

$$|\mathcal{T}_\mathrm{x}| = \prod_{\substack{i=0 \\ p_i \leftarrow p_{i,t}}}^{L-1} p_i \tag{12}$$

and in $\mathcal{R}_\mathrm{x}$ respectively

$$|\mathcal{R}_\mathrm{x}| = \prod_{\substack{i=0 \\ p_i \leftarrow p_{i,r}}}^{L-1} p_i. \tag{13}$$

Each number in $\mathcal{T}_\mathrm{x}$ is used as a position coordinate for one transmitter antenna in the MIMO design. In the same way, the elements of $\mathcal{R}_\mathrm{x}$ are used as coordinates for the receiving antennas. A MIMO system can have at most one distinct VE location for each Tx-Rx pair. Hence, the number of VEs is limited to $|\mathcal{T}_\mathrm{x}| \cdot |\mathcal{R}_\mathrm{x}| = N_\mathrm{Tx} \cdot N_\mathrm{Rx} = L$ in the design method introduced here. Therefore, the separation into Tx and Rx antennas is feasible, as it is capable of producing a MIMO array according to Eq. (3).

All physical antennas lie on a line parallel to the x-axis at y_Tx for Tx and y_Rx for Rx respectively. Consequently, every element of the VA is located along y at

$$y_\mathrm{VA} = \frac{y_\mathrm{Tx} + y_\mathrm{Rx}}{2}. \tag{14}$$

The same applies to the x-coordinate for each possible Tx-Rx pair. The spatial scaling of $\frac{1}{2}$ will be irrelevant for the following argument and will hence be disregarded. Each element in $\mathcal{T}_\mathrm{x}$ and $\mathcal{R}_\mathrm{x}$ determines the x-coordinate of one antenna according to

$$x = 2k \cdot \mathtt{conv}(d; S), \tag{15}$$

where k denotes the scaling factor from Eq. (3). The VA returned from the Tx and Rx positions, which are now fully determined, satisfies the required form from Eq. (3). This can be seen, when the sum of the x-components of Rx and Tx is performed in the domain of number system S. Any element a in $\mathcal{T}_\mathrm{x}$ with symbols t_i added to any element b in $\mathcal{R}_\mathrm{x}$ with symbols r_i yields a decimal result

$$\begin{aligned} \mathtt{conv}(a; S) + \mathtt{conv}(b; S) &= t_{W-1} + \sum_{i=0}^{W-2} t_i \\ &\cdot \left(\prod_{j=i+1}^{W-1} \alpha_j \right) + r_{W-1} + \sum_{i=0}^{W-2} r_i \cdot \left(\prod_{j=i+1}^{W-1} \alpha_j \right) \\ &= [t|r]_{W-1} + \sum_{i=0}^{W-2} [t|r]_i \cdot \left(\prod_{j=i+1}^{W-1} \alpha_j \right). \end{aligned} \tag{16}$$

Table 1. Elements of $\mathcal{T}_\mathrm{x}$ and $\mathcal{R}_\mathrm{x}$ for the first example with $\mathcal{P}_1 = \langle 2_r, 3_t, 5_r, 2_t \rangle$.

$\mathcal{T}_\mathrm{x}$ (in S)	$\mathcal{T}_\mathrm{x}$ (decimal)	$\mathcal{R}_\mathrm{x}$ (in S)	$\mathcal{R}_\mathrm{x}$ (decimal)
0000	0	0000	0
0001	1	0010	2
0100	10	0020	4
0101	11	0030	6
0200	20	0040	8
0201	21	1000	30
–	–	1010	32
–	–	1020	34
–	–	1030	36
–	–	1040	38

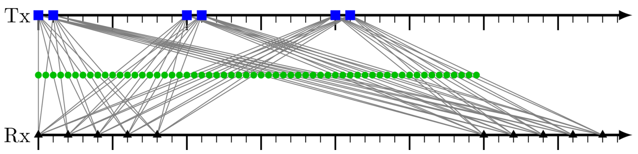

Figure 2. Positioning of Tx (blue squares) and Rx (black triangles) antennas along a number line originating from $\mathcal{P}_1$. The resulting virtual elements are shown as green circles.

This simplification can be done due to the way, $\mathcal{T}_\mathrm{x}$ and $\mathcal{R}_\mathrm{x}$ are defined. For each digit, either the symbol t_i or r_i is zero. When computing the sum in S, no carry events are happening and through the enumeration, each number in S is reached exactly once through the combination of each one element from $\mathcal{T}_\mathrm{x}$ and $\mathcal{R}_\mathrm{x}$. Therefore, the set of all Tx-Rx combinations yields $\mathbb{S}_S$. It follows that a VE for a particular position along the x-axis is generated from exactly one Tx-Rx pair.

3.3 Design examples

To illustrate the working principle of this design concept, two different examples are shown that generate a VA with size $L = 60$. More examples and a more small-step explanation of the method can be found in Holder and Eberspächer (2022). The prime factors $\{2, 2, 3, 5\}$ of L can be ordered and assigned with the subscripts t or r arbitrarily. For the first run,

$$\mathcal{P}_1 = \langle 2_r, 3_t, 5_r, 2_t \rangle \tag{17}$$

is chosen. The used number system is $S_1 = \langle 2, 3, 5, 2 \rangle$. The elements of $\mathcal{T}_\mathrm{x}$ and $\mathcal{R}_\mathrm{x}$ are given in S and as decimals in Table 1.

As a second possible assignment,

$$\mathcal{P}_2 = \langle 2_t, 5_r, 2_t, 3_t \rangle \tag{18}$$

is chosen. The used number system here is $S_2 = \langle 2, 5, 2, 3 \rangle$. The elements of $\mathcal{T}_\mathrm{x}$ and $\mathcal{R}_\mathrm{x}$ for this second example are given in Table 2.

Table 2. Elements of $\mathcal{T}_\mathrm{x}$ and $\mathcal{R}_\mathrm{x}$ for the second example with $\mathcal{P}_2 = \langle 2_t, 5_r, 2_t, 3_t \rangle$.

$\mathcal{T}_\mathrm{x}$ (in S)	$\mathcal{T}_\mathrm{x}$ (decimal)	$\mathcal{R}_\mathrm{x}$ (in S)	$\mathcal{R}_\mathrm{x}$ (decimal)
0000	0	0000	0
0001	1	0100	6
0002	2	0200	12
0010	3	0300	18
0011	4	0400	24
0012	5	–	–
1000	30	–	–
1001	31	–	–
1002	32	–	–
1010	33	–	–
1011	34	–	–
1012	35	–	–

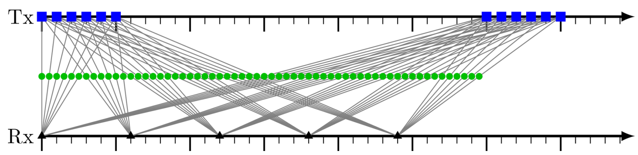

Figure 3. Positioning of Tx (blue squares) and Rx (black triangles) antennas along a number line originated from $\mathcal{P}_2$. The resulting virtual elements are shown as green circles.

Figures 2 and 3 show the generated distributions of antennas and their VA for the two exemplary assignments of $\mathcal{P}$. The first distribution, derived from $\mathcal{P}_1$ in Eq. (17), has six Tx antennas divided into three groups of two. The reason for this structure are the elements 2_t and 3_t in $\mathcal{P}_1$. The second example has 12 Tx antennas and reveals a completely different structure in Fig. 3. The choice of $\mathcal{P}$ influences the balance between the number of Tx and Rx and gives the designer some freedom about structuring the antennas into groups. This could be used to meet other design constraints, like a minimum distance between two receivers or minimum total space occupation. A smaller number of Tx antennas facilitates finding a set of orthogonal waveforms. Lockwood et al. (1996) created several MIMO arrays of same size to compare their radiation pattern and beamforming capabilities. However, the uniform MIMO arrays in the paper are just given as examples without any claim about completeness or source. Therefore, a nomenclature is introduced in the following section to properly classify the possible arrays.

3.4 Nomenclature

In the previous sections, a design method for equidistant and equally weighted MIMO arrays was introduced. The designer has two degrees of freedom when deciding for a sequence $\mathcal{P}$ of subscripted prime factors: The order of the prime factors and their individual assignment to Tx (t) or Rx (r). To classify this design freedom, a nomenclature is proposed. The chain of characters

$$[T|R]_{x_0}[T|R]_{x_1}\ldots[T|R]_{P-1} \tag{19}$$

uniquely identifies a MIMO array. The letter R or T determines, whether this prime factor is assigned to r or t. The subscripts x_i give the number system S. Adjacent digits with the same assignment can be accumulated in one digit with a base corresponding to the product of the individual bases, e.g. the subsequence R_3R_2 will result in the same virtual array as R_2R_3 or R_6. To avoid this ambiguity, each basis should be accumulated such that T and R appear in an alternating fashion. So, the array descriptor $T_2T_2R_5R_3T_3$ should be converted to $T_4R_{15}T_3$ to increase readability. In favor of generality, arrays with only one Tx or one Rx can be notated as T_nR_1 or R_nT_1 respectively. Although strictly speaking they are not MIMO arrays.

3.5 Shifting lemma

Independent of the designed array, shifting all Rx by a spatial vector $\mathbf{s}_{\mathrm{Rx}}$ or all Tx by $\mathbf{s}_{\mathrm{Tx}}$ does not affect the structure of the VA. Tx and Rx positions (encoded as a vector $\boldsymbol{p} = (x, y)^T$ here)

$$\boldsymbol{p}'_{\mathrm{Rx},i} = \boldsymbol{p}_{\mathrm{Rx},i} + \mathbf{s}_{\mathrm{Rx}}; \qquad \boldsymbol{p}'_{\mathrm{Tx},j} = \boldsymbol{p}_{\mathrm{Tx},j} + \mathbf{s}_{\mathrm{Tx}} \tag{20}$$

are each shifted by an offset vector. The VA itself is just displaced by the arithmetic mean of $\mathbf{s}_{\mathrm{Tx}}$ and $\mathbf{s}_{\mathrm{Rx}}$ since the resulting position

$$\boldsymbol{p}'_{\mathrm{VA};i,j} = \boldsymbol{p}_{\mathrm{VA};i,j} + \frac{\mathbf{s}_{\mathrm{Tx}} + \mathbf{s}_{\mathrm{Rx}}}{2}, \tag{21}$$

of the VE is shifted by the same amount for each $i < N_{\mathrm{Rx}}$ and $j < N_{\mathrm{Tx}}$.

4 Example design for a two-dimensional array

The concept of continuously building up antenna groups through digit assignment can also be implemented for the case of a 2D MIMO. In order to create a regular MIMO array in two dimensions, one could either make use of a square grid or a hexagonal grid. A comparison is given by Wagner et al. (2018). Dahl et al. (2017) investigated fractal design approaches on a hexagonal grid, which as well are structured methods to design MIMO arrays of arbitrary size. In this paper, a square grid is used to enable the use of fourier based 3D imaging algorithms (Sheen et al., 2001). For this, the method introduced in the previous section is applied to the vertical and horizontal direction separately. A more practical example is shown using a 80 GHz radar chip.

The goal is to create a 2D MIMO array with the AWR2243 radar transceiver IC from Texas Instruments Incorporated (2020). The chip operates from 76 GHz up to 81 GHz using the FMCW principle. It has three Tx and four Rx channels suitable for MIMO operation. Additionally, multiple chips can be coherently cascaded to operate with an even larger number of antennas. In this example, three chips are used to create an effective size 9 × 12 MIMO array. To get an array size of $L_x = 12$ and $L_y = 9$, the pattern $R_2T_3R_2$ is used in horizontal and T_3R_3 in vertical direction. As the produced MIMO array is intended for *direction of arrival* (DOA) estimation (Chen et al., 2010), a maximum scaling factor of $k = \lambda/4 \approx 3.8$ mm (at center frequency) is allowed theoretically, in order to avoid aliasing. As shown by Zhuge and Yarovoy (2011), this constraint can be relaxed for radar systems with very high fractional bandwidth. The scaling factor $k \approx 2$ mm is defined through Eq. (15) since the availible bandwidth is low. The result is shown in Fig. 4. The shifting property from Eq. (21) is used obtain a symmetric design with a common centroid layout. The next step would be to design a patch antenna and to place it at the positions for Rx and Tx. The microstrip routing to the three chips should then be convenient, as the Tx antennas are already clustered in groups of three.

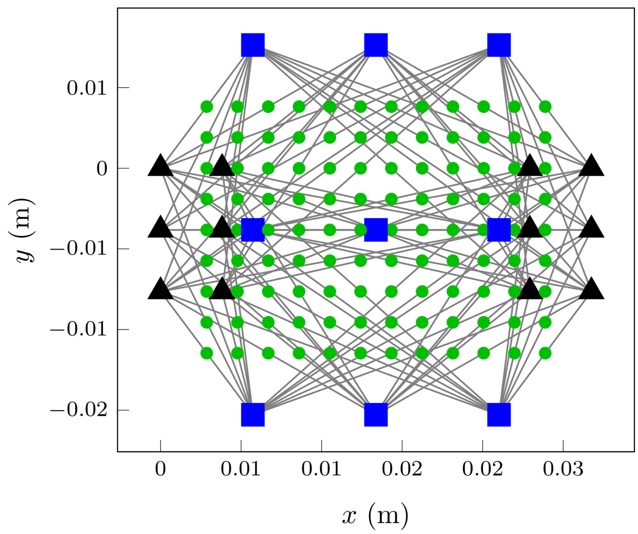

Figure 4. 2D MIMO array design example. Tx positions (blue squares), Rx positions (black triangles) and resulting VA (green circles).

A drawback of this placement choice is that Rx and Tx antennas are close together in the middle row. Populated with patch antennas, this small physical distance would lead to unwanted crosstalk. Alternatively, Tx and Rx could be separated on the circuit board as shown in Fig. 5 by using the shifting property. This leads to larger overall space requirements, but helps reducing crosstalk. Another solution could be to increase the scaling factor k, if the application can implicitly rule out ambiguities from aliasing by design.

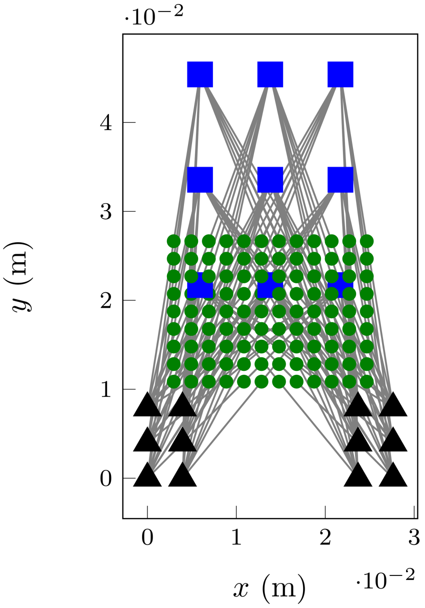

Figure 5. Spatially expanded version of the 2D MIMO array design example. Tx positions (blue squares), Rx positions (black triangles) and resulting VA (green circles) are shown.

4.1 Analysis of published arrays

Numerous other publications already proposed MIMO arrays, which can be created with this method. Zhuge and Yarovoy (2012) are using a 2D array ($R_2T_3R_2$ in both vertical and horizontal direction) as a reference for sparse MIMO near-field imaging investigations. Ender and Klare (2009) use an ARTINO type MIMO array in the form $T_2R_{44}T_{16}$, which is installed along the wings of an aeroplane. Another example is a slightly stretched version of a $T_2R_{16}T_8$ array (Herschel et al., 2016) for a passenger security system.

5 The usage of transceiver antennas

This section describes the special case when TRx antennas are used instead of distinct Tx and Rx. First, an alternative view to convolution and scaling, namely polynomial multiplication is introduced.

5.1 Polynomial multiplication

The concept of polynomial multiplication is not only applicable to TRx antennas, but also distinct Tx and Rx, as in Sect. 3. If Tx and Rx antennas are located on a uniform grid with a defined zero-location, the VA can also be calculated via polynomial multiplication. The set of Tx antennas is therefore expressed as a polynomial $t(x)$. A coefficient c_i is either 1, if a transmitter antenna is present at this grid point or 0, if not. From the example in Fig. 2, $t(x) = 1 + x + x^{10} + x^{11} + x^{20} + x^{21}$ would be returned, while $r(x) = 1 + x^2 + x^4 + x^6 + x^8 + x^{30} + x^{32} + x^{34} + x^{36} + x^{38}$ would describe the Rx positions.

The occuring exponents show where Tx antennas are located. The same applies to Rx yielding a second polynomial $r(x)$ with binary coefficients d_j. The VA is now computed via polynomial multiplication as

$$v(x) = t(x) \cdot r(x) = \sum_{i=0}^{\deg(t(x))} \sum_{j=0}^{\deg(r(x))} c_i d_j x^{i+j}, \tag{22}$$

where $\deg(\cdot)$ denotes the degree of a polynomial. The exponent of a term in $v(x)$ indicates the position of the VE while the corresponding coefficient shows, how many Tx-Rx pairs contribute to it. As for the convolution method, the VA has to be spatially scaled by $\frac{1}{2}$. However, the scaling is not relevant for analyzing the structure of the VA.

5.2 Structured approach for TRx MIMO arrays

If instead of dedicated transmitters and receivers, transceivers are used, the initially proposed methology still works but leads to more redundancy. When each antenna is used as Tx and Rx (TRx), there is no difference between Tx and Rx anymore. This can be understood with the thought, that the sets $\mathcal{T}_\mathrm{x}$ and $\mathcal{R}_\mathrm{x}$ now consist of the set unions

$$\mathcal{T}_\mathrm{x}' = \mathcal{R}_\mathrm{x}' = \mathcal{T}_\mathrm{x} \cup \mathcal{R}_\mathrm{x} \tag{23}$$

of the initial sets.

The obtained VA from a given regular antenna layout can be represented as the result of a polynomial multiplication. Since the antennas are indistinguishable, $t(x) = r(x) = a(x)$ holds, where $a(x)$ denotes a polynomial encoding of the TRx positions. Given that the VA is now calculated as

$$v(x) = (a(x))^2. \tag{24}$$

It can be seen from any TRx structure with $N_\mathrm{TRx} \geq 2$ antennas, that redundancy is now implicitly present. The VA originated from two TRx antennas has the form

$$v(x) = \left(1 + x^k\right)^2 = 1 + 2x^k + x^{2k} \tag{25}$$

for an arbitrary positive integer k. The value 2 in the cross-term coefficient shows, that this structure already contains redundancy as two VEs overlay each other at this position.

Let a TRx array with polynomial $a(x)$ have degree n. This means the rightmost TRx element is at position n and the highest nonzero term of $a(x)$ is x^n. Assume that the resulting VA does not have any gaps, i.e. $v_i \geq 1$ for $i \in [0, 2n]$ holds for the coefficients v_i of $v(x)$. Now consider an extended TRx array, which is composed of $a(x)$ and a shifted copy of $a(x)$. It has the form $a_e(x) = a(x) + x^{2n+1} \cdot a(x)$. The resulting extended VA has the form

$$v_e(x) = (a_e(x))^2 = a(x)^2 \cdot \left(1 + 2x^{2n+1} + x^{4n+2}\right). \tag{26}$$

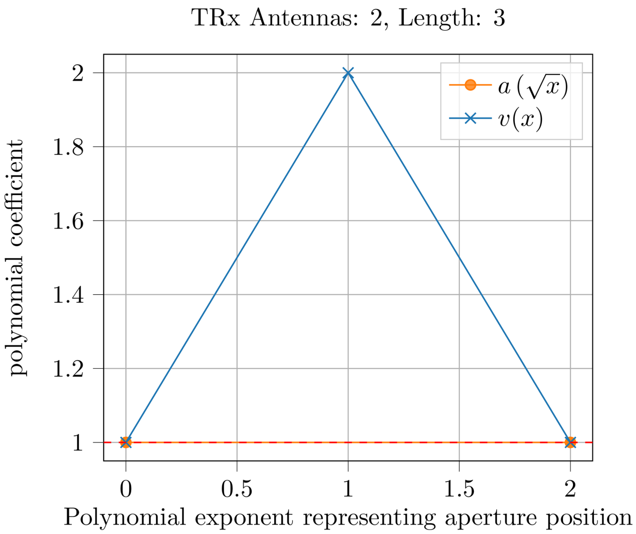

Figure 6. Coefficients of the polynomials $a(x) = 1 + x$ and $v(x) = 1 + 2x + x^2$ for $N_{\text{iter}} = 1$ in Algorithm 1.

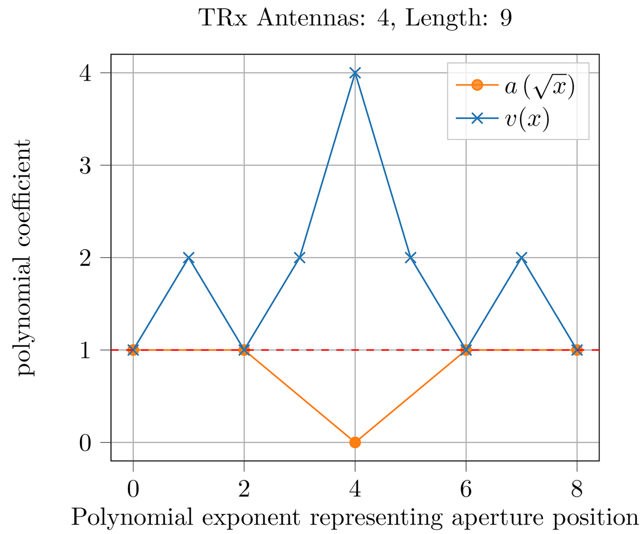

Figure 7. Coefficients of the polynomials $a(x) = 1+x+x^3+x^4$ and $v(x) = 1+2x+x^2+2x^3+4x^4+2x^5+x^6+2x^7+x^8$ for $N_{\text{iter}} = 2$ in algorithm 1.

Since $a(x)^2$ covers all VE positions from zero up to $2n$, the second and third term fully cover the positions ranging from $2n+1$ to $4n+1$ and from $4n+2$ to $6n+2$, respectively. By copying and shifting the existing structure, the VA can be extended to three times the original length. This step can be cascaded several times to build up a large VA. The following iterative procedure illustrates this: The first iteration starts with a single TRx antenna represented by a polynomial $a_0(x) = 1$ of degree zero. Algorithm 1 shows the procedure to get the TRx MIMO array.

Algorithm 1 Iterative method to design a TRx MIMO array.

$a(x) \leftarrow 1$
$n \leftarrow 0$
for i from 1 to N_{iter} **do**
  $a_e(x) = a(x) + x^{2n+1}a(x)$
  $a(x) \leftarrow a_e(x)$
  $n \leftarrow 3n+1$
end for

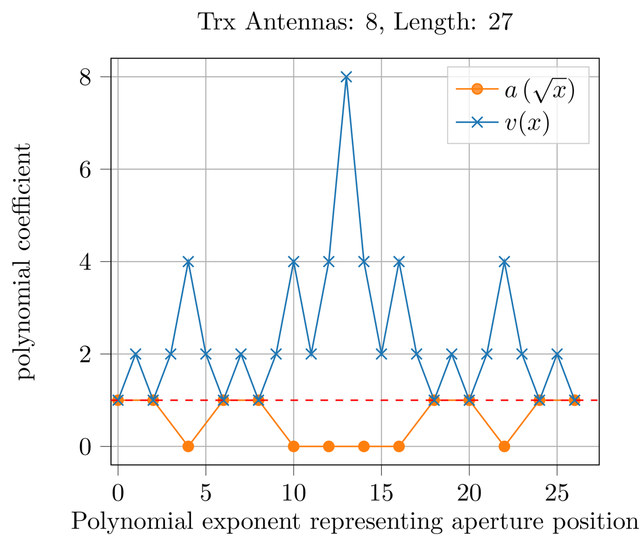

Figure 8. Coefficients of the polynomials $a(x)$ and $v(x)$ for $N_{\text{iter}} = 3$ in algorithm 1.

Figures 6 and 7 show the results for $N_{\text{iter}} = 1$ and $N_{\text{iter}} = 2$ of Algorithm 1. Note that the coefficients of $a(x)$ are shown at stretched positions to visualize the scaling effect, when the VA is generated. Figures 8 and 9 show the coefficients for $N_{\text{iter}} = 3$ and $N_{\text{iter}} = 4$, respectively. It can be observed that the coefficients get larger over the iterations. While the number of TRx doubles, the MIMO array length is multiplied by three for each iteration.

Compared to the number approach of the previous sections, there are fundamental differences: The redundancy for TRx arrays does increase with the N_{iter}, whereas the number approach was designed to not permit redundancy at all. In exchange, the TRx arrays rely on strictly repeating structures, which lowers the hardware complexity. If the spacing is not feasible inside one iteration, one could always use a smaller shift between the two subarrays to get $a_e(x)$. For the iteration, the alternatively produced $a(x)$ from the previous iteration could be used without problems. Additionally, the physical size of the VA coincides with the extent of TRx antennas. For the number system approach, this is never the case.

For a selection of N antennas, the theoretical maximum size L for a regular VA without gaps is $\frac{N\cdot(N+1)}{2}$ for TRx elements. If the antennas are distinct transmitters or receivers, it is $\frac{N^2}{4}$. So roughly half of the size is achieved compared to TRx for large N. While the number system approach reaches

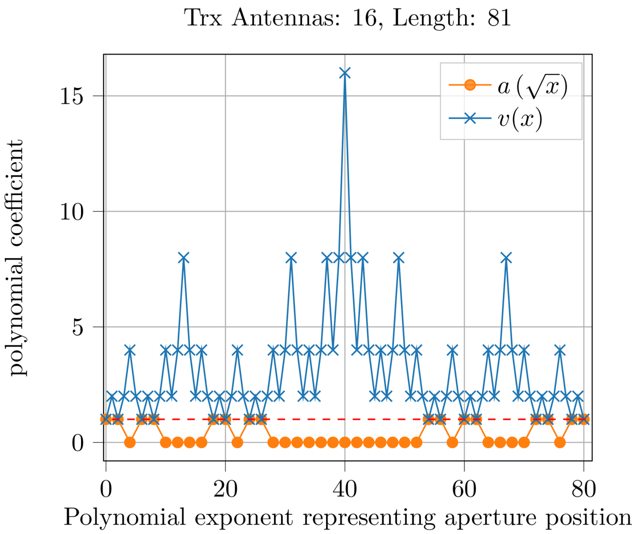

Figure 9. Coefficients of the polynomials $a(x)$ and $v(x)$ for $N_{\text{iter}} = 4$ in Algorithm 1.

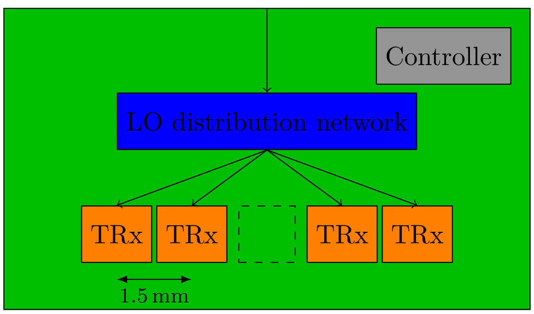

Figure 10. Block diagram of a module using 4 TRx.

this limit asymptotically, the outlined approach for TRx elements still has room for improvement.

5.3 Design example

One significant benefit of the approach followed is the resulting modularity of the system. To demonstrate this advantage, a conceived design example is presented in this section. Consider a modular system design, where 16 TRx are used in four modules with four antennas per module. They are operating at a center frequency of 200 GHz. To achieve a sampling density of $\lambda/2$ of the VA at the center frequency, the minimum distance between two TRx is set to 1.5 mm. The transmitter of each TRx can be deactivated to be operated as a receiver only. With only one active transmitter at a time, TDM could be easily realized. Figure 10 shows an outline of such a submodule. It has four TRx antennas arranged in a grid of five with a void element in the middle. Note that this is exactly the obtained structure for $N_{\text{iter}} = 1$ in Algorithm 1, shown in Fig. 7.

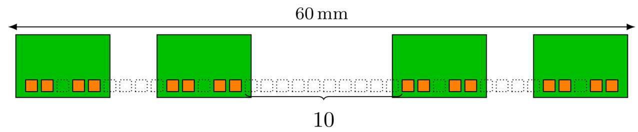

Figure 11. Block diagram of a module using 4 TRx.

These modules are now placed onto a carrier frame with an arrangement as shown in Fig. 11. First (corresponding to iteration 3 in Algorithm 1) the second module is placed with four units of free space next to the leftmost one. This structure is copied again at the right side. Note, that the free space in the middle is only 10 units wide. However, according to Algorithm 1, it should be 13. It was reduced here to meet an overall maximum length constraint of 60 mm. The resulting VA is therefore reduced in size from 81 to 75. Being able to reduce the shifting distance during one iteration is another benefit of this approach, which increases the flexibility during the design process.

6 Conclusions

In this paper, two design methods for creating uniform and equidistant MIMO arrays for 1D and 2D applications were introduced. A nomenclature to classify the degrees of freedom in the first method was proposed. Based on a design example for a 2D MIMO array, the versatility of this method was demonstrated. This was underlined by already published designs of other authors, which all could be created with the introduced design method. As a special case, a design method with TRx antennas was introduced and compared. It was shown that redundant virtual elements are implicitly present in this case.

On the other hand, the examples also highlighted limitations of the methods. Design goals and constraints like the physical size of an antenna (and therefore the minimum spacing) or routing constraints are not implicitly considered. Moreover, the special interest of the authors lies in the application of a MIMO structure for near-field imaging. Zhuge and Yarovoy (2011) point out that array factors are position dependant and more complex to determine in a near field scenario, which will be considered in future work. Removing the constraint of equal weighting in the VA, one could either choose to design redundant arrays ($L < N_{\text{VE}}$), sparse arrays ($L > N_{\text{VE}}$) or a combination of both. Both options will be considered in the near future, investigating the effect of an array choice on the realisability and performance of the radar. Especially, the use of a non-convex optimization algorithm lies in the interest of the authors. Another aim of the authors is to find a more elegant and flexible way to design TRx MIMO arrays. A non-trivial two-dimensional extension of the introduced TRx method must be found as well.

Data availability. No data sets were used in this article.

Author contributions. Both authors conceptualized the ideas of this work. MH carried out the formal analysis and elaborated the methology. He drafted and prepared the manuscript including the visualization of data. ME supervised the work, validated the concepts, reviewed and edited the paper draft.

Competing interests. The contact author has declared that none of the authors has any competing interests.

Disclaimer. Publisher's note: Copernicus Publications remains neutral with regard to jurisdictional claims in published maps and institutional affiliations.

Special issue statement. This article is part of the special issue "Kleinheubacher Berichte 2022". It is a result of the Kleinheubacher Tagung 2022, Miltenberg, Germany, 27–29 September 2022.

Acknowledgements. The authors would like to thank the innovation department of Balluff GmbH for general support and resource provision for this work.

Review statement. This paper was edited by Thomas Kleine-Ostmann and reviewed by two anonymous referees.

References

Chen, Z., Gokeda, G., and Yu, Y: Introduction to Direction-of-Arrival Estimation, Artech house, Norwood, Massachusetts, 46 pp., ISBN 9781596930902, 2010.

Dahl, C., Rolfes, I., and Vogt, M.: Investigation of fractal MIMO concepts for radar imaging of bulk solids, in: 2017 European Radar Conference (EURAD), 134–137, https://doi.org/10.23919/EURAD.2017.8249165, 2017.

Ender, J. H. G. and Klare, J.: System architectures and algorithms for radar imaging by MIMO-SAR, in: 2009 IEEE Radar Conference, 1–6, https://doi.org/10.1109/RADAR.2009.4976997, 2009.

Feger, R., Wagner, C., Schuster, S., Scheiblhofer, S., Jager, H., and Stelzer, A.: A 77-GHz FMCW MIMO Radar Based on an SiGe Single-Chip Transceiver, IEEE T. Microw. Theory, 57, 1020–1035, https://doi.org/10.1109/TMTT.2009.2017254, 2009.

Gao, J., Qin, Y., Deng, B., Wang, H., and Li, X.: Novel Efficient 3D Short-Range Imaging Algorithms for a Scanning 1D-MIMO Array, IEEE T. Image Process., 27, 3631–3643, https://doi.org/10.1109/TIP.2018.2821925, 2018.

Herschel, R., Lang, S. A., and Pohl, N.: MIMO imaging for next generation passenger security systems, in: Proceedings of EUSAR 2016: 11th European Conference on Synthetic Aperture Radar, 1–4, ISBN 978-3-8007-4228-8, 2016.

Holder, M. and Eberspächer, M.: A versatile method to design an equidistant MIMO array, in: 2022 Kleinheubach Conference, 1–4, ISBN 978-3-948571-07-8, 2022.

Huang, Y., Ma, L., Yu, X., Zhang, H., Li, J., and Xi, X.: MIMO Antenna Array Design Based on Genetic Algorithm, in: 2021 IEEE 4th International Conference on Electronic Information and Communication Technology (ICEICT), 406–409, https://doi.org/10.1109/ICEICT53123.2021.9531259, 2021.

Krieger, G., Gebert, N., and Moreira, A.: Multidimensional Waveform Encoding: A New Digital Beamforming Technique for Synthetic Aperture Radar Remote Sensing, IEEE T. Geosci. Remote Sens., 46, 31–46, https://doi.org/10.1109/TGRS.2007.905974, 2008.

Lockwood, G., Li, P.-C., O'Donnell, M., and Foster, F.: Optimizing the radiation pattern of sparse periodic linear arrays, IEEE T. Ultrason. Ferr., 43, 7–14, https://doi.org/10.1109/58.484457, 1996.

Schmid, C. M., Feger, R., Wagner, C., and Stelzer, A.: Design of a linear non-uniform antenna array for a 77-GHz MIMO FMCW radar, in: 2009 IEEE MTT-S International Microwave Workshop on Wireless Sensing, Local Positioning, and RFID, 1–4, https://doi.org/10.1109/IMWS2.2009.5307896, 2009.

Sheen, D., McMakin, D., and Hall, T.: Three-dimensional millimeter-wave imaging for concealed weapon detection, IEEE T. Microw. Theory, 49, 1581–1592, https://doi.org/10.1109/22.942570, 2001.

Chen, C. and Vaidyanathan, P. P.: MIMO Radar Spacetime Adaptive Processing and Signal Design, in: MIMO radar signal processing, edited by: Stoica, P. and Li, J., J. Wiley & Sons, Hoboken, New Jersey, 238–242, ISBN 9780470391488, 2009.

Texas Instruments Incorporated: AWR2243 product page, https://www.ti.com/product/AWR2243 (last access: 26 January 2023), 2020.

Wagner, J., Barowski, J., Dahl, C., and Rolfes, I.: Comparison between Rectangular and Hexagonal Synthetic Apertures for Radar Imaging, in: 2018 15th European Radar Conference (EuRAD), 150–153, https://doi.org/10.23919/EuRAD.2018.8546654, 2018.

Yanik, M. E. and Torlak, M.: Near-Field MIMO-SAR Millimeter-Wave Imaging With Sparsely Sampled Aperture Data, IEEE Access, 7, 31801–31819, https://doi.org/10.1109/ACCESS.2019.2902859, 2019.

Yanik, M. E., Wang, D., and Torlak, M.: Development and Demonstration of MIMO-SAR mmWave Imaging Testbeds, IEEE Access, 8, 126019–126038, https://doi.org/10.1109/ACCESS.2020.3007877, 2020.

Zhuge, X. and Yarovoy, A. G.: A Sparse Aperture MIMO-SAR-Based UWB Imaging System for Concealed Weapon Detection, IEEE Trans. Geosci. Remote Sens., 49, 509–518, https://doi.org/10.1109/TGRS.2010.2053038, 2011.

Zhuge, X. and Yarovoy, A. G.: Study on Two-Dimensional Sparse MIMO UWB Arrays for High Resolution Near-Field Imaging, IEEE T. Antenn. Propag., 60, 4173–4182, https://doi.org/10.1109/TAP.2012.2207031, 2012.